Infrared magneto-optical and photoluminescence studies of the electronic properties of In(As,Sb) strained-layer superlattices

S. R. Kurtz and R. M. Biefeld
Sandia National Laboratories, Albuquerque, New Mexico 87185
(Received 25 January 1991)

Long-wavelength magnetotransmission and photoluminescence measurements were performed on $InAs_{0.13}Sb_{0.87}$/InSb strained-layer superlattices (SLS's). The energies and reduced effective masses of several interband optical transitions were obtained from these experiments. SLS's with different layer thicknesses produced self-consistent results. With these data, the type-II band offset and band-edge strain-shift parameters were accurately determined. Consistent with a type-II offset, an extremely small, in-plane effective-mass hole ground state was observed, thus proving that the hole quantum well is located in the biaxially compressed, InSb layer. Nonparabolicity, suggesting valence-band anticrossing, was also observed.

I. INTRODUCTION

There have been few attempts to "band-gap engineer" In(As,Sb) semiconductors although the electronic properties of these materials suggest that In(As,Sb) heterostructures will display novel physical properties and lead to important device applications. $InAs_xSb_{1-x}$ alloys have the smallest band gaps and effective masses among the III-V semiconductors. Low-dimensionality effects should be quite pronounced in In(As,Sb) structures. In(As,Sb) may prove useful for high-speed devices, and this system is an obvious starting point to extend the optical response of III-V semiconductors to longer wavelength for infrared detectors and lasers.

In this paper we report on a magneto-optical and photoluminescence study of the electronic and optical properties of $InAs_xSb_{1-x}$ strained-layer superlattices (SLS's). Osbourn first proposed $InAs_xSb_{1-x}$ SLS's for long-wavelength, III-V detectors based on calculations of the electronic properties of strained $InAs_1Sb_{1-x}$,[1] and in previous work, we demonstrated prototype infrared detectors fabricated from these structures.[2,3] Because long-wavelength infrared response was observed at low As content in these SLS's, we concluded that a type-II (or staggered) band offset occurs in the In(As,Sb) system.[4,5] Detailed information obtained from the present study enables us to test and refine our model of the $InAs_xSb_{1-x}$ SLS heterostructure.

The type-II offset should lead to novel valence-band properties. Based on $\mathbf{k}\cdot\mathbf{p}$ theory, $InAs_xSb_{1-x}$ SLS holes should exhibit an in-plane effective mass that is lower than that reported for ground-state holes in any other III-V structure. The hole effective mass should approach that of the InSb conduction band, $0.014m_0$. This "light" hole state should be well separated in energy from the heavier-hole states at higher energy in the valence band. The valence-band electronic properties could be utilized to produce high-speed, p-channel devices and to reduce Auger recombination in infrared lasers.

II. EXPERIMENTAL PROCEDURES

$InAs_{0.13}Sb_{0.87}$/InSb SLS's were grown using metalorganic chemical vapor deposition. The samples were very high quality, essentially free of dislocations and cracks. The SLS's were grown on top of a linearly composition-graded, $InAs_xSb_{1-x}$ alloy strain-relief buffer on a p^--type, InSb substrate. The alloy buffer layer was 2 μm thick. SLS composition, layer thickness, and residual strain were determined using x-ray and transmission electron micrograph analysis described previously.[6] The results of this characterization for two samples with the same nominal composition and different layer thicknesses are shown in Table I. The samples are identified by their approximate layer thicknesses. The total thicknesses of the 100- and 250-Å SLS's are 4.77 and 5.28 μm, respectively. The x-ray strain is defined as $\zeta=(a_\parallel-a_0)/a_0$, where $a_\parallel$ is the SLS lattice constant in the plane and a_0 is the substrate lattice constant. The x-ray strain values in Table I reveal that a small residual strain is present in these SLS's from growing on the lattice-mismatched substrate.

Sample heating and background radiation distort long-wavelength emission spectra, even with careful subtraction procedures. To improve upon results obtained in earlier studies,[5] infrared photoluminescence was measured using a double-modulation experiment. The double-modulation technique provides higher sensitivity, reduces sample heating, and eliminates the blackbody background from infrared emission spectra. The sample was optically pumped with a cw, multimode CO waveguide laser (5.5 μm), and the laser light was chopped at high frequency with an acousto-optic modulator. The infrared luminescence was measured with a Fourier-transform infrared (FTIR) spectrometer equipped with a $Hg_{1-x}Cd_xTe$ detector. The chopped luminescence signal was demodulated with a broadband lock-in amplifier placed between the $Hg_{1-x}Cd_xTe$ detector and the analog to digital (A/D) converter in the FTIR spectrometer.

TABLE I. X-ray characterization of the composition and structure of the $InAs_xSb_{1-x}$ SLS's.

SLS	$InAs_{1-x}Sb_x$ layer x	$InAs_{1-x}Sb_x$ layer Thickness (Å)	InSb layer thickness (Å)	X-ray strain ζ
100 Å	0.871±0.01	96±3	104±3	−0.0035±0.0003
250 Å	0.865±0.01	251±6	258±6	−0.0040±0.0004

This initial demodulation produced a conventional interferogram that was Fourier transformed (equivalent to a second demodulation) to produce an infrared luminescence spectrum. In order to detect radiation in the spectral region of interest, care had to be taken to ensure that the bandwidths of the lock-in and the FTIR overlap.

Low-temperature infrared absorption and magneto-transmission measurements were made with both the sample and a Ge:Cu photoconductive detector immersed in liquid He (4.1 K) in a superconducting magnet cryostat. Infrared light pipes were used to guide radiation from the FTIR spectrometer to the sample and detector. All measurements were made with the magnetic field normal to the SLS planes and unpolarized infrared light at normal incidence to the planes of the SLS (Faraday configuration). The sample was mounted on a carousel, and three wafers could be mounted at one time for comparative studies. To eliminate changes in detector response with magnetic field, the detector was positioned in a field-free region generated by compensation coils built into the superconducting magnet.

III. RESULTS

Low-temperature (4.1 K) infrared absorption spectra for these SLS's are shown in Fig. 1. To correct for surface reflection and ensure that the absorption spectra are characteristic of the SLS, substrate and strain-relief buffer contributions have been subtracted from these spectra. The onset of optical absorption in these SLS's occurs at noticeably lower energy than band gap of the unstrained $InAs_{0.13}Sb_{0.87}$ constituent (≈ 180 meV). These two absorption spectra are quantum-size shifted relative to each other, and several absorption edgelike features, corresponding to optical transitions involving various quantum confinement states, are observed in each spectrum. Comparing the spectra in Fig. 1, the magnitude of the lowest-energy absorption edge increases with decreasing layer thickness. This feature and the "soft" shape of the absorption edges, approximating $(\omega-\omega_0)^{3/2}$, are characteristic of type-II, interband transitions.[7]

The double-modulation technique described earlier was used to obtain infrared photoluminescence spectra shown in Figs. 2 and 3. The photoluminescence intensity was roughly proportional to CO laser pump power over the narrow range (1.4–0.2 W/cm^2 average power) where photoluminescence could be observed. At the higher laser powers, multiple photoluminescence peaks can be resolved. The energies of the photoluminescence peaks correspond to edges in the absorption spectra (Fig. 1). At low pump power, the linewidth of the main photoluminescence peak was 11 and 18 meV fullwidth at half maximum for the 250- and 100-Å SLS's, respectively. As stated in previous publications,[4,5] the lowest-energy transitions observed in the photoluminescence and absorption spectra occur at significantly lower energy than the strain-shifted, low-energy transitions occurring in type-I SLS's with these compositions and layer thicknesses. Therefore, these $InAs_xSb_{1-x}$ SLS's must have a type-II band offset that results in "spatially indirect," low-energy

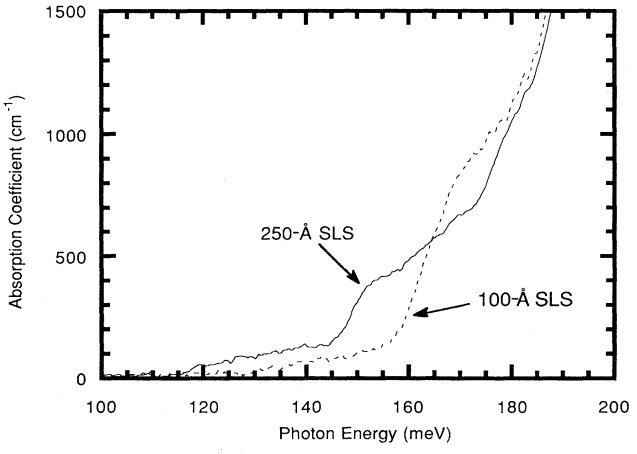

FIG. 1. Infrared absorption spectra for the 100-Å (dotted line) and 250-Å (solid line) $InAs_{0.13}Sb_{0.87}$/InSb SLS's at 4.1 K ($B=0$).

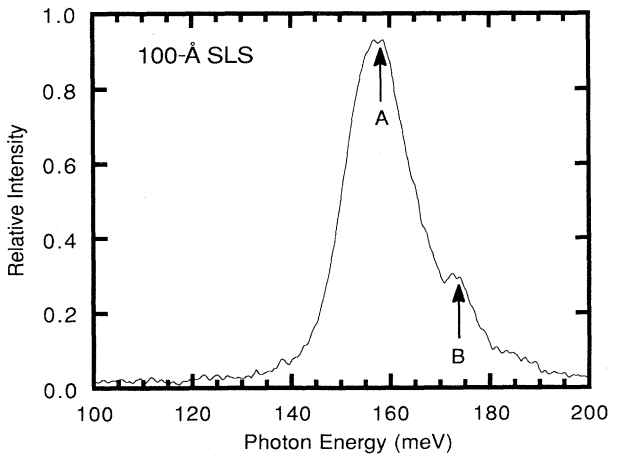

FIG. 2. Photoluminescence spectrum for the 100-Å SLS with a sample temperature of 15 K ($B=0$).

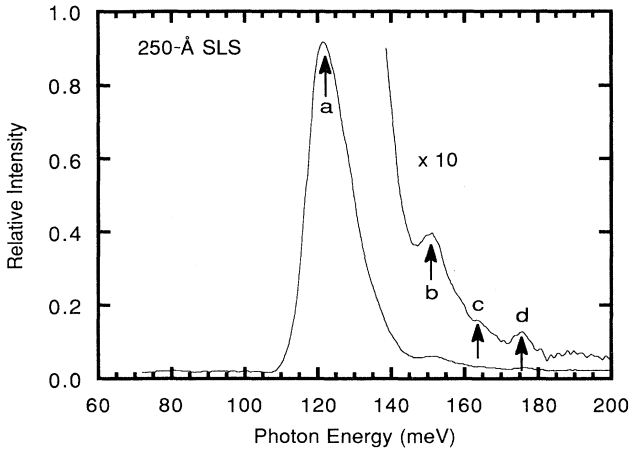

FIG. 3. Photoluminescence spectrum for the 250-Å SLS with a sample temperature of 15 K ($B=0$).

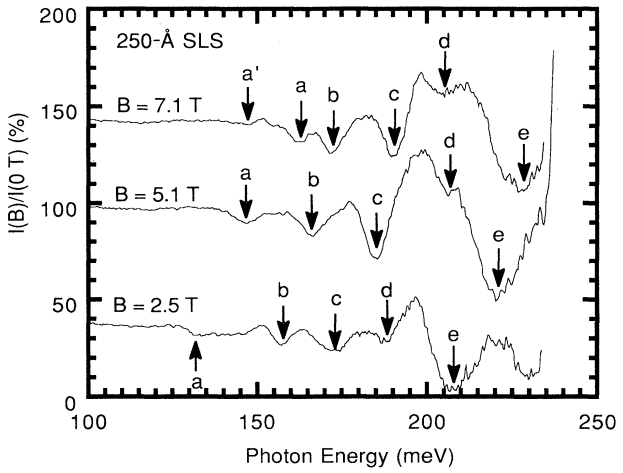

FIG. 5. Magnetotransmission spectra for the 250-Å SLS at 4.1 K, $B=2.5$, 5.1, and 7.5 T.

optical transitions.

Infrared magnetotransmission experiments were performed to identify the multiple transitions observed in photoluminescence and absorption and to study the in-plane electronic properties of these SLS's. At magnetic fields >0.5 T, maxima appear in the interband absorption corresponding to the quantum confinement states each splitting into series of Landau levels. Fortunately, interpretation of the data is simplified because only a few interband magneto-optical transitions are strong enough to be observed experimentally. Landau levels are clearly observed as minima in the ratio of the transmitted intensity at field B and zero field $[I(B)/I(0)]$. Magneto-optical transmission spectra for the 100- and 250-Å SLS's are shown in Figs. 4 and 5 for several magnetic fields. Major transitions in these spectra (indicated in Figs. 2–7) can be followed over a wide range in magnetic field. The quantum-size shift between the 100- and 250-Å SLS's and increasing transition energies with increasing field are apparent in the magneto-optical spectra.

The magnetic-field dependence of the magneto-optical transitions is shown in Figs. 6 and 7 for the 100- and 250-Å SLS's, respectively. The near-linear field dependence justifies semiempirical analysis of the data within the effective mass approximation, and the magneto-optical transitions display different dE/dB values corresponding to different effective masses and various fan diagram lines. All of the transitions observed as photoluminescence peaks are seen in the magneto-optical spec-

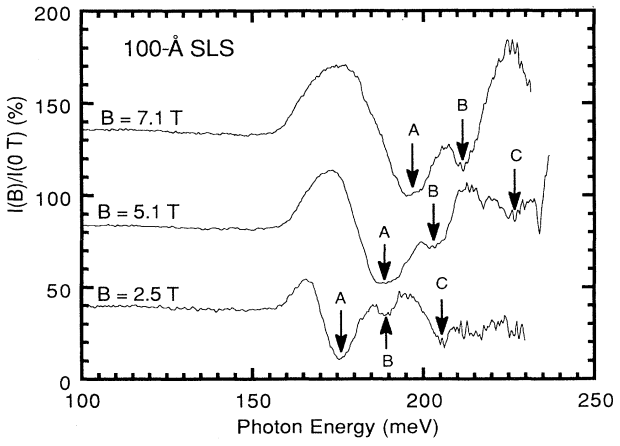

FIG. 4. Magnetotransmission spectra for the 100-Å SLS at 4.1 K, $B=2.5$, 5.1, and 7.5 T.

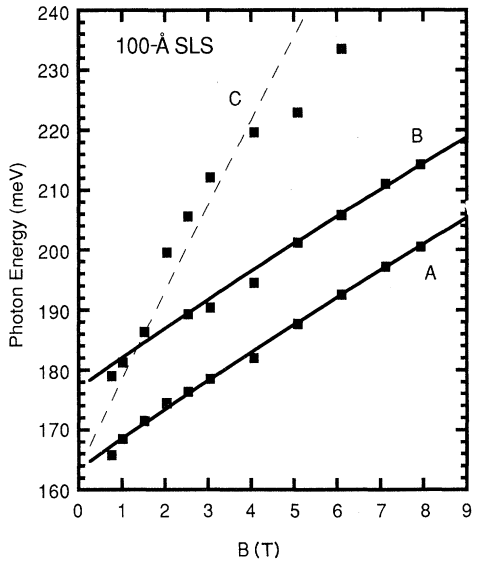

FIG. 6. Magneto-optical peak energies vs magnetic field for the 100-Å SLS. Major $n=0$ transitions are described by a reduced mass of $0.011m_0$ (solid lines). The predicted energy of an $n=1$ transition is indicated by the light dotted line.

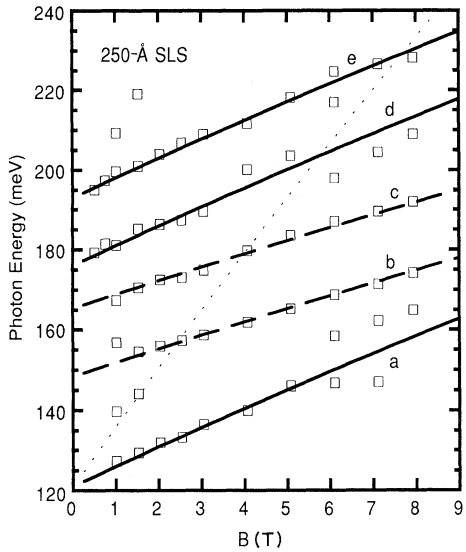

FIG. 7. Magneto-optical peak energies vs magnetic field for the 250-Å SLS. Major $n=0$ transitions are described by reduced-mass values, $0.011m_0$ (solid lines) and $0.016m_0$ (bold dashed lines). The predicted energy of an $n=1$ transition is indicated by the light dotted line.

tra. Fitting these data to a linear field dependence, one finds that the zero-field magnetotransmission energies are in excellent agreement with the photoluminescence peak positions. Magnetic Landau peaks are broadened in other SLS's displaying superior photoluminescence linewidth (≤ 10 meV), and it is difficult to observe magneto-optical transitions corresponding to the main photoluminescence peak. We speculate that shallow impurities may be dominating luminescence and transport in those SLS's.

IV. DATA ANALYSIS

A. $InAs_xSb_{1-x}$ SLS heterostructure and quantum confinement

The multiple optical transitions observed through photoluminescence and magneto-optical studies provide an opportunity for detailed modeling of the heterostructure of $InAs_xSb_{1-x}$ SLS's. The optical data are analyzed by first calculating the strain-induced energy shifts for each layer of the SLS using deformation potentials found in the literature, strain and composition data from Table I, and Vegard's law. For a biaxially strained, direct-gap semiconductor with [001] uniaxial strain, the energies of the conduction band (e) and out-of-plane light-hole (L) and heavy-hole (H) bands are[8]

$$E_e = E_{\text{gap}}(x) + a_c\left[2-2\frac{C_{12}}{C_{11}}\right]\varepsilon_{\parallel}\ , \tag{1}$$

$$E_H = \left[-a_v\left[2-2\frac{C_{12}}{C_{11}}\right]+b\left[1+2\frac{C_{12}}{C_{11}}\right]\right]\varepsilon_{\parallel}\ , \tag{2}$$

$$E_L = \left[-a_v\left[2-2\frac{C_{12}}{C_{11}}\right]-b\left[1+2\frac{C_{12}}{C_{11}}\right]\right]\varepsilon_{\parallel} + \frac{9b^2(1+2C_{12}/C_{11})^2\varepsilon_{\parallel}^2}{4\Delta_0}\ , \tag{3}$$

where $\varepsilon_{\parallel}$ is the biaxial strain in the (001) plane, and $E_{\text{gap}}(x)$ is the unstrained band gap. The sum of the conduction- and valence-band hydrostatic deformation potentials a ($a=a_c+a_v$), the shear deformation potential b, and elastic constants C_{mn}, are estimated from pressure data on bulk InSb and InAs[1,9,10]

$$a=-6.0-1.7x\ , \tag{4}$$

$$b=-1.8-0.25x\ , \tag{5}$$

$$C_{11}=0.6652x+0.8465(1-x)(10^{12}\ \text{dyn/cm}^2)\ , \tag{6}$$

$$C_{12}=0.3351x+0.5001(1-x)(10^{12}\ \text{dyn/cm}^2)\ , \tag{7}$$

where $InAs_{1-x}Sb_x$ is the composition of a SLS layer, and Δ_0 is the Γ_7-Γ_8 split-off energy,

$$\Delta_0(x)=0.81x+0.38(1-x)\ \text{eV}\ . \tag{8}$$

The low-temperature $InAs_{1-x}Sb_x$ band gap is[1,5]

$$E_{\text{gap}}(x)=0.233x^2-0.0363x(1-x)+0.420(1-x)^2\ \text{eV}\ . \tag{9}$$

Generally, $a_c > a_v$, and we assume $a_v \approx 0.1a_c$.[11]

Using the strain-shifted band energies for each SLS component, SLS quantum confinement state energies were calculated for different band offset values using an envelope function model which corrects for band nonparabolicity.[12] Where appropriate, out-of-plane ($\hat{z}$) band-edge effective masses of strained layers scale with the strained band gap from bulk InSb values. (In units of the free electron mass,

$$m^*_{L,z}=m^*_{e,z}=0.014E_{\text{gap}}(x)/(233\ \text{meV}),\quad m^*_{H,z}=0.4\ .)$$

From this study and from preliminary results on SLS's with much higher As content,[13] we find that an unstrained, $InAs_{1-x}Sb_x$ valence-band energy of $(0.36\pm0.04\ \text{eV})x$ produces an offset that satisfactorily describes optical data for SLS's in much of the InAs/InSb system. The resulting unstrained valence-band offset in the $InAs_{0.13}Sb_{0.87}$/InSb structure is 47 meV (type II). This determination of the band offset is reasonably accurate because the band offset term is larger than any strain shifts in these $InAs_{0.13}Sb_{087}$/InSb SLS's, and the band offset is substantially larger than the uncertainties in the strain shifts. The predicted energies of several transitions between quantum confinement states in these SLS's and experimental photoluminescence peaks and magneto-optical transitions are listed in Table II. Agreement with the data is quite good considering that this model has one adjustable parameter, the band offset. Improved agreement could be obtained by fine tuning deformation potentials and effective masses within acceptable limits.

The quantum-well structure of an $InAs_{0.13}Sb_{0.87}$/InSb SLS predicted by the deformation potentials and offset is shown in Fig. 8. The offset between the strained conduction-band minima was found to be 158 meV. Both the heavy- and light-hole quantum wells occurs in the InSb layer (type-II offset). The heavy hole has a significant energy barrier of 75 meV, but the light-hole energy barrier is quite small, 6 meV. The heavy- and

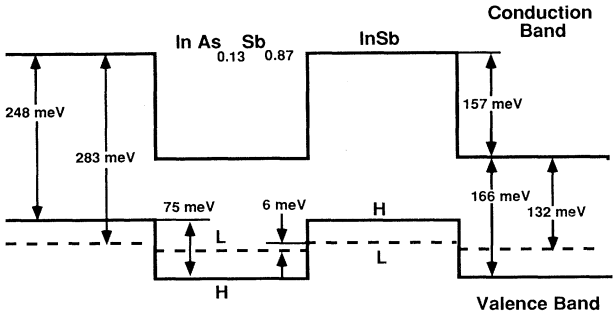

FIG. 8. Quantum-well energies (0 K) of a free standing ($\zeta=-0.0042$) $InAs_{0.13}Sb_{0.87}$/InSb SLS. Out-of-plane heavy-hole H and light hole L wells are indicated. Quantum confinement states have been omitted from the drawing.

light-hole states in the SLS valence band are well separated in energy with the heavy-hole states strongly bound and the light-hole states being essentially continuum states.

B. Magnetic-field effects and in-plane SLS electronic properties

Application of a magnetic field perpendicular to the SLS planes splits each quantum confinement state (i) into a series of Landau levels ($n=0,1,2,\ldots$). The energy levels in the conduction band become

$$E_i(B)=E_i(0)+(n+\tfrac{1}{2})\hbar\omega_c \ , \tag{10}$$

where $\hbar\omega_c$ is the appropriate electron cyclotron frequency. $E_i(0)$ is the $k_\perp=0$ quantum confinement state energy. Assuming isotropic effective mass, the cyclotron frequency is given by

$$\hbar\omega_c=\frac{e\hbar B}{m^*c} \ , \tag{11}$$

where B is the magnetic field, and m^* is an effective mass. With a weak Coulomb interaction,[14] the $\Delta n=0$ selection rule is obeyed, and the interband transitions energies become

$$E_{ij}=E_{ij}(0)+(n+\tfrac{1}{2})\frac{e\hbar B}{\mu_{ij}c} \ , \tag{12}$$

where μ_{ij} is the reduced effective mass,

$$\mu_{ij}=\left[\frac{1}{m_i^*}+\frac{1}{m_j^*}\right]^{-1} . \tag{13}$$

m_i^* and m_j^* are in-plane conduction- and valence-band effective masses. From Eqs. (12) and (13), constant electron and hole effective masses result in a fan of interband magneto-optical transition energies increasing linearly with magnetic field and originating from each $k_\perp=0$ transition with energy $E_{ij}(0)$.

Examining the results in Figs. 6 and 7, we find most of the magneto-optical data correspond to $n=0$ transitions with $\mu=0.011\pm0.001$ (solid lines) or $\mu=0.016\pm0.002$ (dashed lines).[15] (All effective masses are in units of the free-electron mass m_0.) Weaker $n\geq 1$ transitions (light dotted lines) appear when not obscured by other transitions. The linewidths of the magneto-optical transitions are comparable to the photoluminescence linewidths for these samples, and generally, spin splittings could not be resolved in the magneto-transmission spectra.

Quantum confinement or uniaxial strain of the SLS produces valence-band effective masses of

$$\begin{aligned} m_{H,z}^*&=\frac{1}{\gamma_1-2\gamma_2}, \quad m_{L,z}^*=\frac{1}{\gamma_1+2\gamma_2} \ , \\ m_{H,\perp}^*&=\frac{1}{\gamma_1+\gamma_2}, \quad m_{L,\perp}^*=\frac{1}{\gamma_1-\gamma_2} \ , \end{aligned} \tag{14}$$

where γ_1 and γ_2 are Luttinger parameters.[8,16] The out-of-plane effective masses are unchanged from their bulk values, but the in-plane heavy-hole effective mass is very light ($m_{H,\perp}^*\approx\frac{4}{3}m_{L,z}^*$).[17] The in-plane light-hole mass ($m_{L,\perp}^*$) is heavier, but it remains significantly lighter than the heavy hole in the bulk. Conduction-band effective masses remain almost isotropic, close to the bulk values.[18] Consistent with our model of the SLS heterojunction, (e-H) transitions correspond to the smaller reduced mass (see Table II and Figs. 6 and 7), and the

TABLE II. Experimental energies and predicted quantum confinement transitions.

		Energy (meV)		SLS heterojunction model	
SLS	Peak	Photoluminescence peak	Magneto-optics transition, $B=0$	Quantum confinement transition	Energy (meV)
250 Å	a	122	121	(1e-1H)	117
	b	151	148	(1e-1L)	153
	c	163	165	(1e-2L)	164
	d	175	177	(2e-1H)	180
	e		194	(1e-ΓH)	191
100 Å	A	158	164	(1e-1H)	163
	B	174	177	(1e-2H)	181

magneto-optical results support the transitions assigned to the photoluminescence peaks. Furthermore, ($1e$-$1H$) is the lowest-energy transition in both of the SLS's. This proves conclusively that the hole quantum well is located in the biaxially compressed InSb layer, and these SLS's have a type-II band offset.

As a starting point for evaluating masses, we can use bulk InSb hole effective masses ($m^*_{H,z}=0.4$, $m^*_{L,z}=0.014$) and Eq. (14) to estimate the in-plane SLS hole masses ($m^*_{H,\perp}=0.018$, $m^*_{L,\perp}=0.051$). Clearly, $m^*_{L,\perp}$ makes a significant contribution to the reduced mass observed for (e-L) transitions, and m_e^*, $m^*_{L,\perp}$, and $m^*_{H,\perp}$ cannot all be determined using only the reduced mass values. A cyclotron resonance study of p-type $InAs_xSb_{1-x}$ SLS's revealed two peaks, and based on those results, we speculate $m^*_{H,\perp}=0.03$ and $m^*_{L,\perp}=0.06$.[19] Using $m^*_{L,\perp}=0.06$ and our measured reduced masses, one obtains $m_e^*=0.022$ and $m^*_{H,\perp}=0.022$. Effective masses determined from cyclotron resonance and interband transmission are in reasonable agreement considering the uncertainties in interpretation of data obtained from few samples.

The $\mathbf{k}\cdot\mathbf{p}$ interaction between quantum confinement states results in complicated behavior of the in-plane effective masses,[20] and in general, these masses are increased by interactions with other subbands. Both the ($1e$-$1H$) and ($2e$-$1H$) transitions deviate from linearity and appear to split at >5 T in Fig. 7. We speculate that this is due to spin splitting or the repulsion of the low-energy heavy-hole state by the higher-energy light-hole state at finite $k_\perp$. Also, the electron and "lightlike" hole in-plane masses (m_e^* and $m^*_{H,\perp}$) are heavier than expected from InSb values and basic $\mathbf{k}\cdot\mathbf{p}$ theory, and within experimental uncertainty, the reduced mass values are surprisingly insensitive to quantum confinement energy $E_i(0)$. A large basis of quantum confinement states, in both the valence and conduction bands, would be needed to model these narrow-band-gap superlattices, and the calculation is clearly beyond the scope of this experimental study.

V. CONCLUSIONS

Infrared photoluminescence and magnetotransmission experiments revealed detailed information about the heterostructure and electronic properties of $InAs_xSb_{1-x}$ SLS's. Quantum-size shifts were observed in a comparison of two SLS's with nominally the same composition, $InAs_{0.13}Sb_{0.87}$/InSb. The multiple optical transitions seen in these SLS's enabled us to determine the band offset with a high degree of accuracy. Based on this study and other SLS's we have measured, the band offset is type II in much of the In(As,Sb) system, and the offset is described by an $InAs_{1-x}Sb_x$ alloy unstrained valence-band energy of $(0.36\pm0.04\text{ eV})x$ eV. With this large type-II offset, optical absorption in $InAs_xSb_{1-x}$ SLS's can be extended to long wavelength at low As concentration, and $InAs_{1-y}Sb_y/InAs_{1-x}Sb_x$ SLS's should display semimetal behavior for $(x-y)>0.3$ and $E_{\text{gap}}(x)>E_{\text{gap}}(y)$. Therefore, very long-wavelength (>12 μm) materials and devices can be constructed with III-V compounds using $InAs_xSb_{1-x}$ SLS's.

The magnetic-field studies confirm our model of the $InAs_xSb_{1-x}$ SLS heterostructure. Reduced-mass values were consistent with our identification of the optical transitions. The lowest-energy optical transitions observed in these SLS's had the smallest in-plane hole masses. Therefore, the lowest-energy interband transitions are (e-H), and the hole quantum well is located in the biaxially compressed InSb layer of the SLS. Most of the data are described by reduced mass values, $\mu=(0.011\pm0.001)m_0$ (e-H) and $\mu=(0.016\pm0.002)m_0$ (e-L). Using these reduced masses to evaluate in-plane SLS effective masses, we find $m_e^*=(0.024-0.016)m_0$ and $m^*_{H,\perp}=(0.021-0.035)m_0$ for a range of $m^*_{L,\perp}$ values, $m^*_{L,\perp}=(0.05-\infty)m_0$. Elevated in-plane masses and nonparabolicity observed at the highest fields are probably caused by anticrossings and interactions between the quantum confinement states at finite $k_\perp$.

$InAs_xSb_{1-x}$ SLS holes display an in-plane effective mass that is lower than that reported for ground-state holes in any other III-V structure. Based on the band offsets and effective masses reported in this work, it should be possible to construct very high-speed p- and n-channel devices using strained $InAs_xSb_{1-x}$ structures. The novel valence band with the "light" hole ground state should result in a reduction of Auger recombination and may lead to improvements in III-V infrared laser performance, equaling that attained with Pb salts.

ACKNOWLEDGMENTS

We thank our colleagues, G. C. Osbourn, E. D. Jones, S. K. Lyo, I. J. Fritz, and L. R. Dawson, for illuminating discussions. D. L. Moore and S. R. Lee provided technical assistance. This work was performed at Sandia National Laboratories, supported by the U.S. Department of Energy under Contract No. DE-AC04-76DP00789.

[1]G. C. Osbourn, J. Vac. Sci. Technol. B **2**, 176 (1984).
[2]S. R. Kurtz, R. M. Biefeld, L. R. Dawson, I. J. Fritz, and T. E. Zipperian, Appl. Phys. Lett. **53**, 1961 (1988).
[3]S. R. Kurtz, L. R. Dawson, T. E. Zipperian, and R. D. Whaley, Jr., IEEE Electron Device Lett. **11**, 54 (1990).
[4]S. R. Kurtz, G. C. Osbourn, R. M. Biefeld, L. R. Dawson, and H. J. Stein, Appl. Phys. Lett. **52**, 831 (1988).
[5]S. R. Kurtz, G. C. Osbourn, R. M. Biefeld, and S. R. Lee, Appl. Phys. Lett. **53**, 216 (1988).
[6]R. M. Biefeld, C. R. Hills, and S. R. Lee, J. Cryst. Growth **91**, 515 (1988).
[7]G. Bastard, *Wave Mechanics Applied to Semiconductor Heterostructures* (Les Editions de Physique, Paris, 1988).
[8]Fred H. Pollak, in *Semiconductors and Semimetals,* edited by R. K. Williamson and A. C. Beer (Academic, New York, 1990), Vol. 32, pp. 17–55, and references therein.
[9]*Numerical Data and Functional Relationships in Science and Technology,* edited by O. Madelung, M. Schulz, and H. Weiss,

Landolt-Börnstein, New Series, Vols. 17a and 17b (Springer, New York, 1982).

[10]G. Simmons and H. Wang, *Single Crystal Elastic Constants and Calculated Aggregate Properties* (MIT, Cambridge, MA, 1971).

[11]C. G. Van de Walle, in *Epitaxy of Semiconductor Layered Structures,* edited by R. T. Tung, L. R. Dawson, and R. L. Gunshor, MRS Symposia Proceedings No. 102 (Materials Research Society, Pittsburgh, 1988), p. 565.

[12]G. Bastard and J. A. Brum, IEEE J. Quantum Electron. **QE-22**, 1625 (1986); G. Bastard, Phys. Rev. B **24**, 5693 (1981).

[13]S. R. Kurtz, L. R. Dawson, and R. M. Biefeld (unpublished).

[14]S. K. Lyo, E. D. Jones, and J. F. Klem, Phys. Rev. Lett. **61**, 2265 (1988).

[15]Reduced masses and $B=0$ transitions were determined from nonlinear curve fits with nonparabolic light masses of the form, $m_i^*(E)=m_i^*\{1+[E-E_i(0)]/E_{\text{gap}}\}$.

[16]G. C. Osbourn, Superlatt. Microstruct. **1**, 223 (1985).

[17]J. E. Schirber, I. J. Fritz, and L. R. Dawson, Appl. Phys. Lett. **46**, 187 (1985).

[18]C. Hermann and C. Weisbuch, Phys. Rev. B **15**, 823 (1977).

[19]S. Y. Lin, D. C. Tsui, L. R. Dawson, C. P. Tigges, and J. E. Schirber, Appl. Phys. Lett. **57**, 1015 (1990). The background doping in the SLS strain-relief buffer is not specified. With a p-type background, tensile strain in the $InAs_xSb_{1-x}$ alloy buffer would produce a second cyclotron resonance peak corresponding to $m_{L,1}^*$.

[20]T. Ando, J. Phys. Soc. Jpn. **54**, 1528 (1985).